energies

MDPI

Article

Efficacy of Green Oxide Nanofluids as Potential Dispersants for Asphaltene in Iraqi Crudes, Experimental, Tunning and Statistical Analysis

Dana Khidhir [1,*] and Hiwa Sidiq [2]

[1] Department of Petroleum Engineering, Faculty of Engineering, Soran University, Soran 44008, Kurdistan Region, Iraq
[2] Department of Petroleum Engineering, Komar University of Science and Technology, Sulaymaniyah 46001, Kurdistan Region, Iraq
* Correspondence: dmk750h@pete.soran.edu.iq

Abstract: Asphaltene are large molecular crude constituents and their existence is related to numerous problems. However, nanofluids have proven to be a very stable and effective way of dealing with asphaltene agglomerations. This research addresses the effectiveness of nanofluids as compared to traditional and available (FLOW-X) commercial inhibitors. The synthesis and characterization of two green NPs and the preparation of nanofluids were performed successfully in this study. It was found that by tuning the concentration of nanofluid, the efficiency increases by 17%. Crude samples have shown different responses to nano inhibitors. It was found that nanofluids increase asphaltene dissolution by nearly 22% as compared to commercial inhibitors.

Keywords: asphaltene; ADT; nanoparticle; inhibitors; nanofluids

Citation: Khidhir, D.; Sidiq, H. Efficacy of Green Oxide Nanofluids as Potential Dispersants for Asphaltene in Iraqi Crudes, Experimental, Tunning and Statistical Analysis. *Energies* **2022**, *15*, 6833. https://doi.org/10.3390/en15186833

Academic Editors: Qiangui Zhang, Xiangyu Fan and Yufei Chen

Received: 29 August 2022
Accepted: 14 September 2022
Published: 19 September 2022

1. Introduction

Asphaltenes are physically coke-like compounds that alkanes can deposit and cause to flocculate [1]. At room temperature, they are largely insoluble in typical paraffins such as *n*-heptane, *n*-hexane, and *n*-pentane, but soluble in toluene or benzene. By studying its structure and how asphaltene behaves in the presence of other hydrocarbon molecules, several researchers have attempted to understand the nature of asphaltene and why it precipitates. SARA analysis, which stands for Saturates, Aromatics, Resins, and Asphaltenes, is one method for calculating the asphaltene content in crude oil by weight percentage [2]. Once pressure, temperature, and compositional changes occur, asphaltene loses its stability, and hence precipitation. It was found that during natural depletion, the amount of precipitated asphaltene increases at the bubble point [3]. These changes affect reservoirs, tubing, facilities for surface production, gas injection, and chemical treatment [4]. Researchers have discovered that the physical characteristics of crude oil can change as a result of asphaltene precipitation [5]. It was discovered that there is an ideal inhibitor concentration that is essential to controlling deposition, using Sodium Dodecyl Sulfate (SDS), X−100, and Salicylic Acid and Naphthalene [6]. The structure of asphaltene inhibitors causes them to function as a bridge between residual oil, which is a non-polar substance, and asphaltene, which is a polar chemical. For example, inhibitors function by joining hydrophilic groups to asphaltene and hydrophobic groups to the remaining oil. TiO_2 (Titanium Oxide nanoparticle) has been discovered to significantly improve asphaltene's stability by creating hydrogen bonds with an acidic medium. Because of their structural makeup, inhibitors serve as a "bridge" between polar (asphaltene) and non-polar (the majority of oil) media, preventing the aggregation of particles by joining hydrophilic groups to asphaltene and hydrophobic groups to the majority of oil TiO_2 [7]. Academics have proposed that the average asphaltene aggregation size is more than 500 nm [8]. During EOR processes,

asphaltene precipitation increases especially with CO_2 injections [9]. The idea of using a nanomaterial in asphaltene inhibition is still modern; however, there has been much evidence showing that using metal oxide NPs will improve and disperse asphaltene. The findings demonstrate that rutile (TiO_2) fine nanoparticles can significantly increase the stability of asphaltene in acidic settings and act in the opposite manner in basic conditions. Metal oxide nanoparticles have a large specific surface area and a strong ability for adsorption. Furthermore, the heteroatoms of oxygen, sulfur, and nitrogen contained in asphaltene molecules can be absorbed by the surface of nanoparticles. By keeping the asphaltene molecules in suspension and protecting them from precipitation and deposition, oil recovery is increased by roughly 8–22% [10] (see Figure 1). Many scholars have studied the application of nanotechnology in terms of (production, EOR, drilling, etc.) [11]. The author in [12] found that asphaltene adsorbs to nickel–zeolite oxide nanoparticles. Based on a number of factors, green technology-produced nanoparticles are considerably better than those produced via physical and chemical processes. For instance, green methods minimize the need for costly chemicals, utilize less energy, and produce products and byproducts that are ecologically friendly. Table 1 demonstrates some of the key findings in modern literature along with the outcomes of each study.

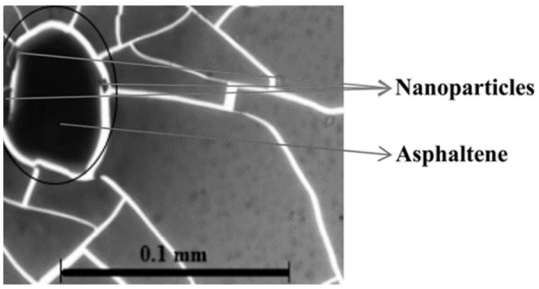

Figure 1. Asphaltene molecule surrounded by Nanoparticles [10].

Table 1. Uses of asphaltene Nano Inhibitors in literature.

Author	*year*	*SARA%*	*API*	*Inhibitor*	*AOS*	*Outcome*
[7]	2017	Asp 8.2%−11.4	22.4 26.7	0.04 wt% (80%TiO_2:20 %SiO_2	production	The onset of asphaltene flocculation (the *n*-heptane volume increased).
[13]	2018	Saturate% 56.2 Aromatic% 34.1 Resin% 7.7 Asphaltene% 2.0	37	CaO 45 ppm SiO2 45 ppm	production/EOR	In wide ranges of data, as temperature increased, asphaltene upper onset pressure increased. CaO and SiO_2 nanoparticles decreased asphaltene precipitations in the presence of CO.
[14]	2017			(Poly (vinyltoluene-co-alpha-methylstyrene)) 6% wt	production	Asphaltene inhibitor makes the asphaltene particles more stable due to its unique ability to interact between asphaltene particles and asphaltene inhibitor molecules via *p*–*p* interactions and hydrogen bonding.
[15]	2011	Asph 10% wt	19	TiO_2 + HNO_3 (65%)	production	Results show that rutile (TiO_2) fine nanoparticles can effectively enhance the asphaltene stability in acidic conditions and act inversely in basic conditions.

Table 1. *Cont.*

Author	*year*	*SARA%*	*API*	*Inhibitor*	*AOS*	*Outcome*
[16]	2020			A, B, C 500 ppm	production	The results show that when an asphaltene inhibitor is not injected into the mixture of synthetic oil/*n*-heptane, AOP (Asphaltene Onset Point) occurs at 35 vol.% of *n*-heptane, while with addition of 3000 ppm of asphaltene B inhibitor, AOP occurs at 60 vol.% of *n*-heptane.
[17]	2019	45.6 41 7.6 5.8	31.7	AI 1, 500 ppm	production	The efficiency of the AI on dispersing the asphaltenes was observed to have a major impact on the precipitation as possibly increasing the deposition of microcrystalline waxes.
[18]	2019	45 16.5 8.5 3 Wax 12	25.03	*n*-phenylamino hexanol	production	Asphaltene deposition in the pores of sandstone core is studied by flooding the virgin and additive beneficiated crude oil indicating less deposition in beneficiated crude oil.
[19]	2012	28.04 21.16 12.48 38.32		SDJ agent 1% wt	production	Colloid instability index greater than 0.9 can effectively inhibit asphaltene deposition in the wellbore.
[20]	2021			CNPs	reservoir	Aggregation of asphaltene can be delayed from 26 to 37% Vol *n*-C7 with the existence of 400 ppm CNPs.

2. Materials and Methods

A precursor of copper chloride ($CuCl_2$), zinc sulfate ($ZnSO_4$), and hydroxide (NaOH) was acquired from Sigma-Aldrich Chemicals Co., Ltd. (Saint Louis, MO, USA) for the synthesis of nanoparticles. In the city of Erbil, Eucalyptus nicholii was gathered from the Soran province region. Two nano metal oxide particles were prepared and then subjected to XRD, SEM, EDX, and UV–Vis spectroscopy for characterization. Methanol, Xylene, and Dichloromethane (DCM) were acquired from Chem-Lab for the nanofluid synthesis. Nine samples were utilized to examine the effectiveness of the nano inhibitor for asphaltene dispersion testing. The samples and their corresponding attributes were gathered from oilfields in Iraq. The wells are producing at depths between 2450 and 3720 m. Due to the confidentiality of the data names, they have been given a different code; the pay zones in these fields are qamchuka, pilaspe, Mishrif, sargalu, Baba, and shiranish. The fields' previously used names have been removed. The fields often have various pay zones that are produced from tertiary and cretaceous formations (upper and lower qamchuka, shiranish) (see Table 2). A commercial inhibitor was procured from an oil field chemical provider in order to compare the findings and the effectiveness of the produced nano-oxide fluid. This inhibitor, known as FLOW-X, is frequently employed in field applications for the dispersion of asphaltene.

Table 2. Crude samples.

Sample	*Sample Point*	*Sp, Gr*	*API*	*Grade*	*Known Asphaltene Problem*
K1	main stream	0.916	23	Medium	Non
K2	well head	0.904	25	Medium	Moderate
K3	well head	0.86	33	Light	Non
K4	well head	0.871	31	light	Moderate
K5	wellhead	0.898	26	Medium	Non
K6	separator	0.84	37	Light	Non
K7	wellhead	0.993	11	U. Heavy	Sever
K8	storage tank	0.887	28	Intermediate	Non
K9	mainstream	0.882	29	Intermediate	Moderate

2.1. Preparation of Eucalyptus Leaf Extract

Eucalyptus Leaf was washed with deionized water to eliminate any contaminants. The leaf was then left to dry for six days in a dark place. By using a grinder and a mortar, the leaf was turned into fine powder. Approximately 100 g of the plant was added to 250 mL of deionized water and heated to 80 °C with continuous stirring for 35 min. The resulting yellow solution was filtered by using Whatman paper at room temperature. The extract was then collected in a 150 mL beaker to be used directly for the syntheses of ZnO and CuO NPs.

2.2. Synthesis of Green CuO and ZnO Nanoparticles

Figure 2 shows the synthesis of ZnO and CuO NPs from copper chloride ($CuCl_2$) and zinc sulfate ($ZnSO_4$). Initially, the extract was heated to 70 °C. Then, at a molarity of 0.1, both metal salts were added dropwise to the plant extract at 60–70 °C while being vigorously stirred, and a (green) solution for ZnO was formed ideally while for CuO NPs, a (dark-green) solution was obtained. The PH level was then raised to 11.8 for CuO NPs and 11.9 for ZnO NPs by adding NaOH solution dropwise since an acidic environment is essential for the formation of nanomaterials. Subsequently, the solution was kept at 75 °C for 45 min; then, the solution was washed with methanol and calcinated in a muffle furnace at 350 °C for three hours. After Calcination, a fine powder was obtained (yellow-grey) ZnO and (Black) for CuO NPs, and sent for characterization.

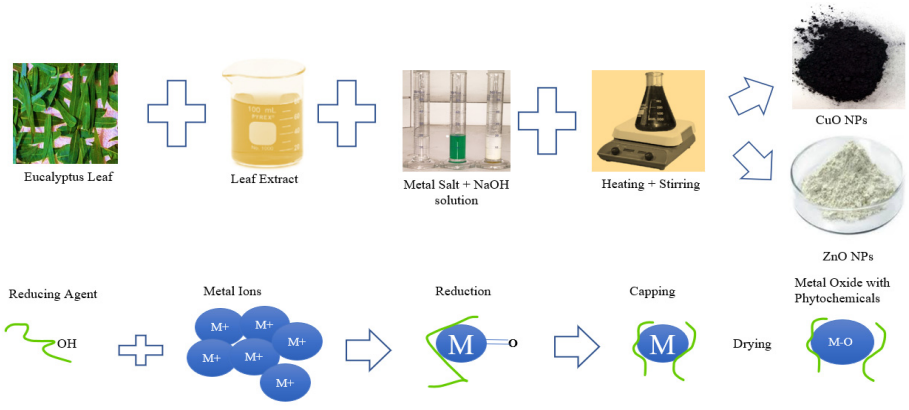

Figure 2. Nanoparticle synthesis steps.

2.3. Syntheses of CuO and ZnO Nonfluids/Chemical

The nanofluid was prepared using Xylene, DBSA, Benzene, Toluene, and DCM. To ensure a thorough dispersion of the nanomaterial, the nanopowder was first dissolved into a combination of DCM (Dichloromethane) and Xylene with continuous stirring for 24 h. The visual approach was employed in periods of 1 and 24 h with various concentrations to test the stability of nanofluids (see Table 3), as detailed more in the sections below.

Table 3. Composition of nonfluids in this study.

Name	*Particle%*	*Xylene%*	*DCM%*	*DBSA%*	*Toluene%*	*Benzene%*
ZnO NF	<1%	15%	40%	2%	17%	25%
CuO NF	<1%	15%	40%	-	19%	25%

2.4. Asphaltene Dispersion Test

Asphaltene Dispersion Test ADT

A modified version of the asphaltene dispersant test was used, which was proposed by [21]. This method is cost-effective, easy, and is used throughout fields as dispersant testing for asphaltene inhibitor efficiency. The test procedure is split into two stages. The first identifies the amount of crude that is required to give a measurable quantity of precipitated asphaltene, and this volume is then used in the second phase to evaluate the performance of the candidate chemicals.

Phase I

Dilute 25 mL of crude with 25 mL of toluene. Shake well to create the oil stock solution and heat to 80 °C until 50% vol is achieved. Add 10 mL of hexane or pentane to each graduated centrifuge tube. Add 50, 150, 200, 250, 300, 400, and 500 µL of the oil stock solution to the centrifuge tubes, shake well, and allow them to stand for two hours. Observe and record the percentage of sedimentation due to gravity. Chose the crude oil dose that gives between 4 and 10% sedimentation after two hours for use in step 2. For the purpose of having a clear baseline, the highest yielding dosage of crude oil was used for all ten samples in this research.

Phase II

Prepare 1% solutions by weight of the dispersants to be evaluated in an appropriate solvent. Thus, 1 ppm will be equivalent to 1 µL of dispersant solution. Add 10 mL of hexane or pentane to the graduated centrifuge tubes. Dose the tubes with the required amount of the dispersant. Typically, the following dose rates are chosen: 0 (blank), 100, 200, and 300 ppm. Shake well. As previously identified in step 1, add the appropriate amount of oil stock solution to each tube. Shake vigorously for 1 min. Allow tubes to stand for two hours (see Figure 3). Observe and record the percentage of sedimentation due to gravity. The percent dispersed is determined by the following formula:

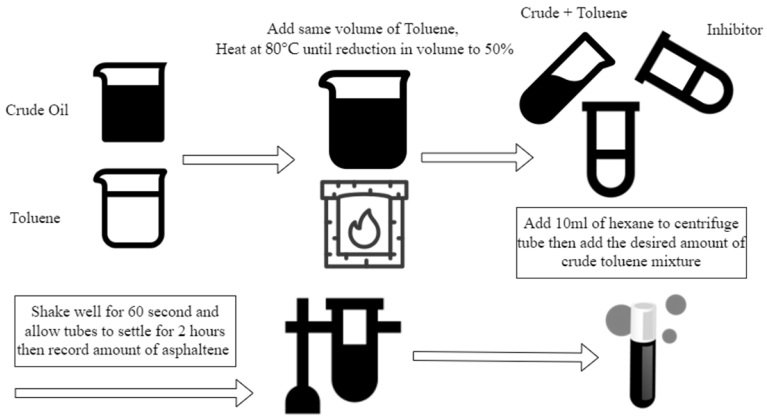

Figure 3. Asphaltene Dispersant Test Procedure.

$\%\ \text{dispersed} = 100\frac{(St-Sb)}{St}$, where St = sediment in treated sample, and Sb = sediment in blank.

2.5. Extraction of Asphaltene

The IP−143 method was used for the determination of crude oil asphaltene content [22]. *n*-Hexane and toluene were used for precipitation and purification of asphaltene, respectively. First, 5 g of crude oil was weighed and mixed with 200 g of *n*-heptane with a

ratio of 1:40 crude to solvent. The first reflux was performed for asphaltene precipitation in crude oil by the *n*-Hexane solvent in the Soxhlet extractor. The primary reflux was performed for 3 h; then, the *n*-hexane/crude oil solution was aged overnight in a dark place. In the second stage, the obtained mixture was filtered using filter paper. The asphaltene and a small number of other components were deposited on the filter paper. The second reflux was performed for separating other components that were bonded in the filter paper by adding *n*-hexane. In the last reflux, asphaltene on the filter paper was separated by adding toluene. Finally, the asphaltene/toluene solution was put under a slow stream of air to evaporate the toluene

3. Results

As shown before, the plant extract was used to synthesize the nanomaterial, and then a stable nanofluid was prepared. The synthesized nanofluid was used as an inhibitor for asphaltene.

3.1. UV–Vis of the Plant Extract

Reduction of Zn and Cu ions was performed by using eucalyptus leaf extract. The important peak was 265, which is an indication of flavonoids [23] whose existence is necessary for the bioreduction of metal salts (see Figure 4).

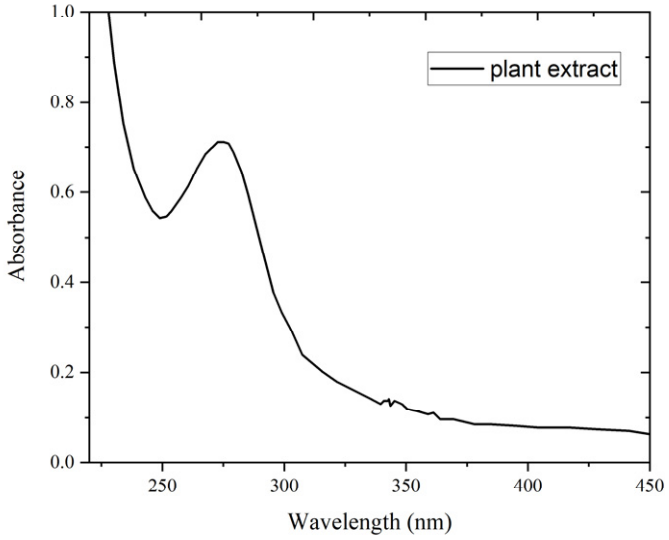

Figure 4. Uv–Vis Leaf Extract.

3.2. FE-SEM, EDX, and Elemental Mapping Analysis

The purity of NPs was investigated using field emission scanning electrons at different magnifications. In both cases for CuO NP and ZnO NPs, the shape of the structures was round and unattached (Figure 5a,b). Note that in CuO NPs, there are some agglomerations in structural shapes. EDX analysis showed very pure Zn, O, and Cu, all of whose peaks were free of any impurities. The chemical elements were investigated using energy dispersive X-ray spectroscopy (EDX) (Figure 5c,d). Almost no impurities were detected and the overall composition of Nio NPs was Ni at 72% and oxygen at 27%, while for ZnO NPs, it was Zn at 75% and oxygen at 24%. In order to improve the quality of the SEM images, NiO NPs were coated with a thin layer of gold, which is why Au can be seen in the EDX spectrum.

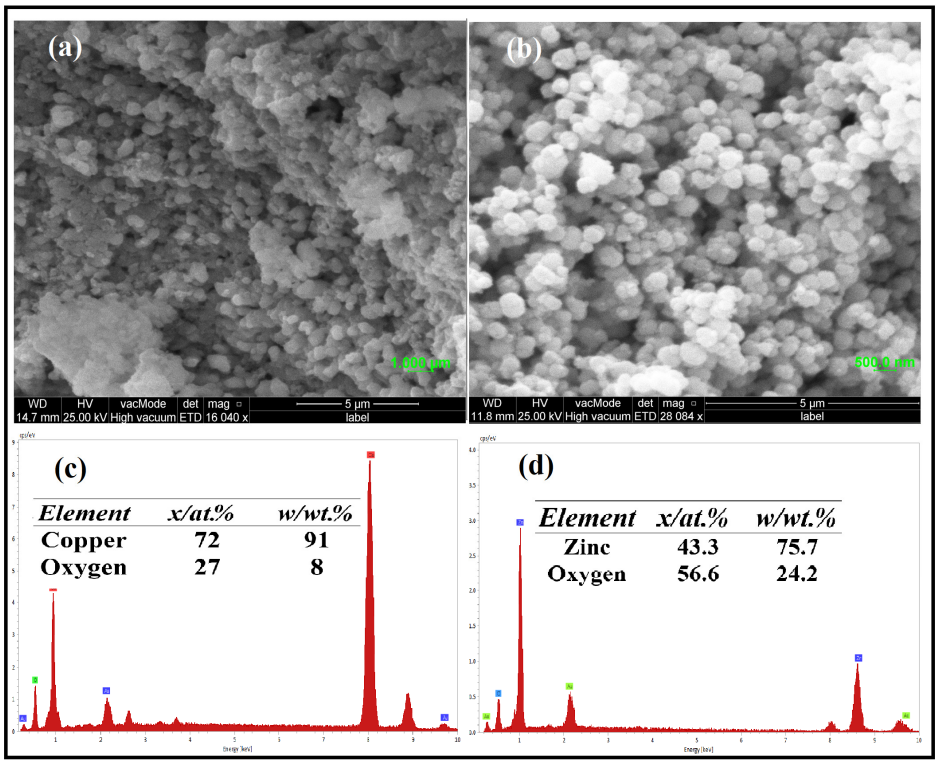

Figure 5. (**a**,**b**) FE-SEM images of CuO and ZnO NPS; (**c**,**d**) EDX spectra of CuO and ZnO NPs.

3.3. X-ray Diffraction (XRD)

Figures 6 and 7 show that an X-ray diffractometer was used to demonstrate the existence of nanoparticles and analyze their structural properties. CuO and ZnO nanoparticles were scanned at 20 to 80 degrees 2 theta in accordance with JSPDS cards 98–006−9758 and 98–005−7478 (Figures 6 and 7). Nanoparticles were recognized and their structural properties were examined using an X-ray diffractometer (Figures 6 and 7). The phytochemicals in plant extract are what cause the oxide peaks. No additional peak is visible in the XRD patterns, which is a clear sign that all precursors and impurities were completely washed and that no impurity peaks were observed by examining the full width at half maximum (FWHM) value of the XRD spectrum. Consequently, the average crystallite size was calculated from the XRD measurement using the Debye–Scherrer equation [24] (Tables 4 and 5). It was found that CuO NPs are 52 nm on average, and ZnO NPs are 20 nm [24,25].

$$D = \frac{0.95\lambda}{\beta D cos\theta} \quad (1)$$

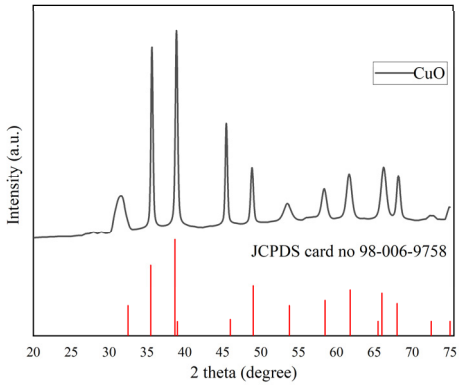

Figure 6. X-ray Diffraction of CuO NPs.

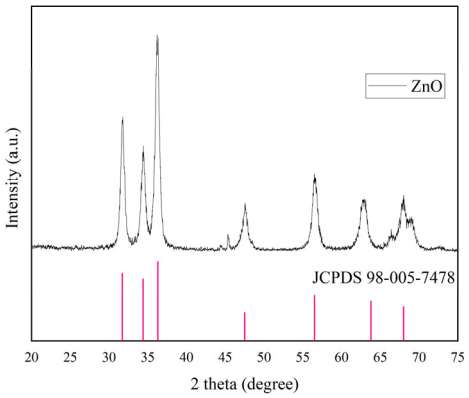

Figure 7. X-ray Diffraction of ZnO NPs.

Table 4. CuO NPs average crystalline size calculation using Debye–Scherrer Equation.

Peak Position 2θ (°)	FWHM B_{size} (°)	D-Spacing (Å)	Dp (nm)
31.2316	0.048	2.86159	179.6245
31.3156	0.036	2.86120	239.5484
31.7262	0.288	2.81810	29.97385
35.6244	0.288	2.51816	30.28406
38.863	0.336	2.31544	26.20617
45.4286	0.288	1.99489	31.25658
48.8144	0.384	1.86414	23.74646
53.4745	1.152	1.71216	8.071059
58.3345	0.768	1.58055	12.38219
61.625	0.768	1.50381	12.58912
66.174	0.768	1.41103	12.90474
68.1274	0.48	1.37525	20.88255
Average FWHM	0.467	Average size	52.2

Table 5. ZnO NPs average crystalline size calculation using Debye–Scherrer Equation.

Peak Position 2θ (°)	FWHM B_{size} (°)	D-Spacing (Å)	Dp (nm)
31.7811	0.2755	2.81569	31.34
34.4442	0.551	2.60384	15.78
36.3632	0.4723	2.47072	18.51
47.5726	0.4723	1.91145	19.21
56.4683	0.4723	1.62963	19.96
62.8988	0.7872	1.47761	12.36
Average FWHM	0.5051	Average size	19.52588

D is the average crystallite size (diameter), λ is the wavelength of the incident X-ray (0.154 nm), θ is Bragg's angle, and βD is full width at half maximum (FWHM).

3.4. Nanofluid Stability

The colloidal stability of nanoparticles was studied by using the visual method. The main goal is to observe for any sedimentation. Copper oxide nanofluid was prepared at 100, 200, 300, and 700 ppm, as mentioned before, and observed for 1 h and 24 h. For the first hour, the nanofluid remained stable and no sedimentation was observed, while after 24 h, some sedimentation was observed for both ZnO and CuO (Figure 8c).

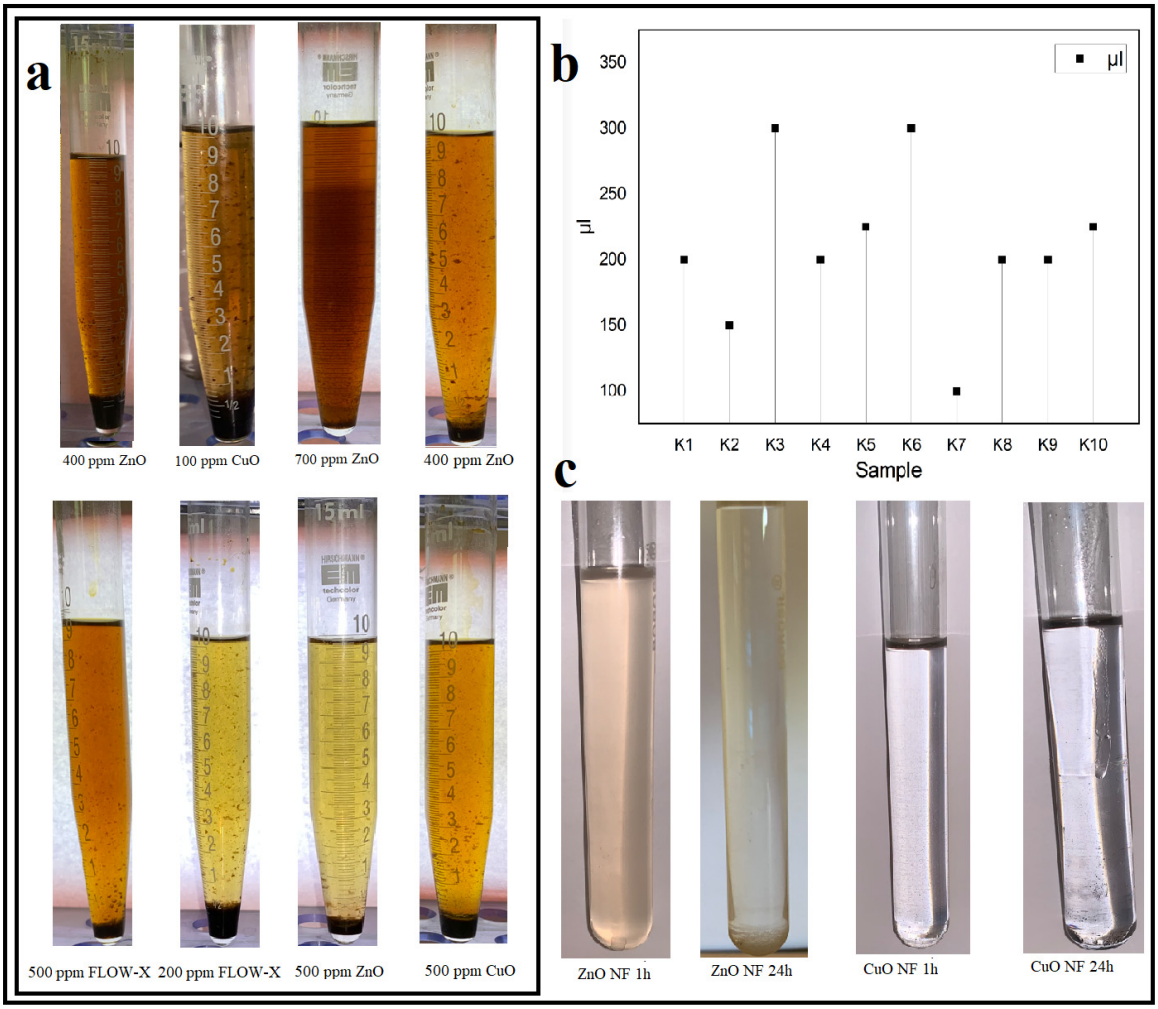

Figure 8. (**a**) ADT test results. (**b**) Blank Test concentration of crude to show 10% precipitation. (**c**) NF stability.

3.5. Asphaltene Dispersion Test

To ensure reliability and reproducibility of the test, each of the nine samples was tested three times and the average was taken. Figure 8a shows the test results as an example. The main difference in preparation for the test was that each of the samples required a certain amount of crude concentration (microliter) to show around 10% precipitation as shown in Figure 8b; for example, K3 required 300 µL of crude to show asphaltene, while some of the crudes showed asphaltene at concentrations of 100–250 µL. For each crude sample, concentrations of 100, 200, and 300–700 ppm were prepared for (CuO NPs, ZnO NPs, and FLOW-X). In general, NPs gave an average improvement over the commercial inhibitor.

3.6. Blank Test Results

Figure 8b shows the results of the ADT control test for asphaltene. It is important to note here that for most of the crude samples, asphaltene precipitation was kept at 10%, which was crucial to determine the efficiency of the chemical inhibitor based on the amount of initial precipitation. While samples K1, K3, and K6 showed a little less than 10% for the given crude volume (Figure 9).

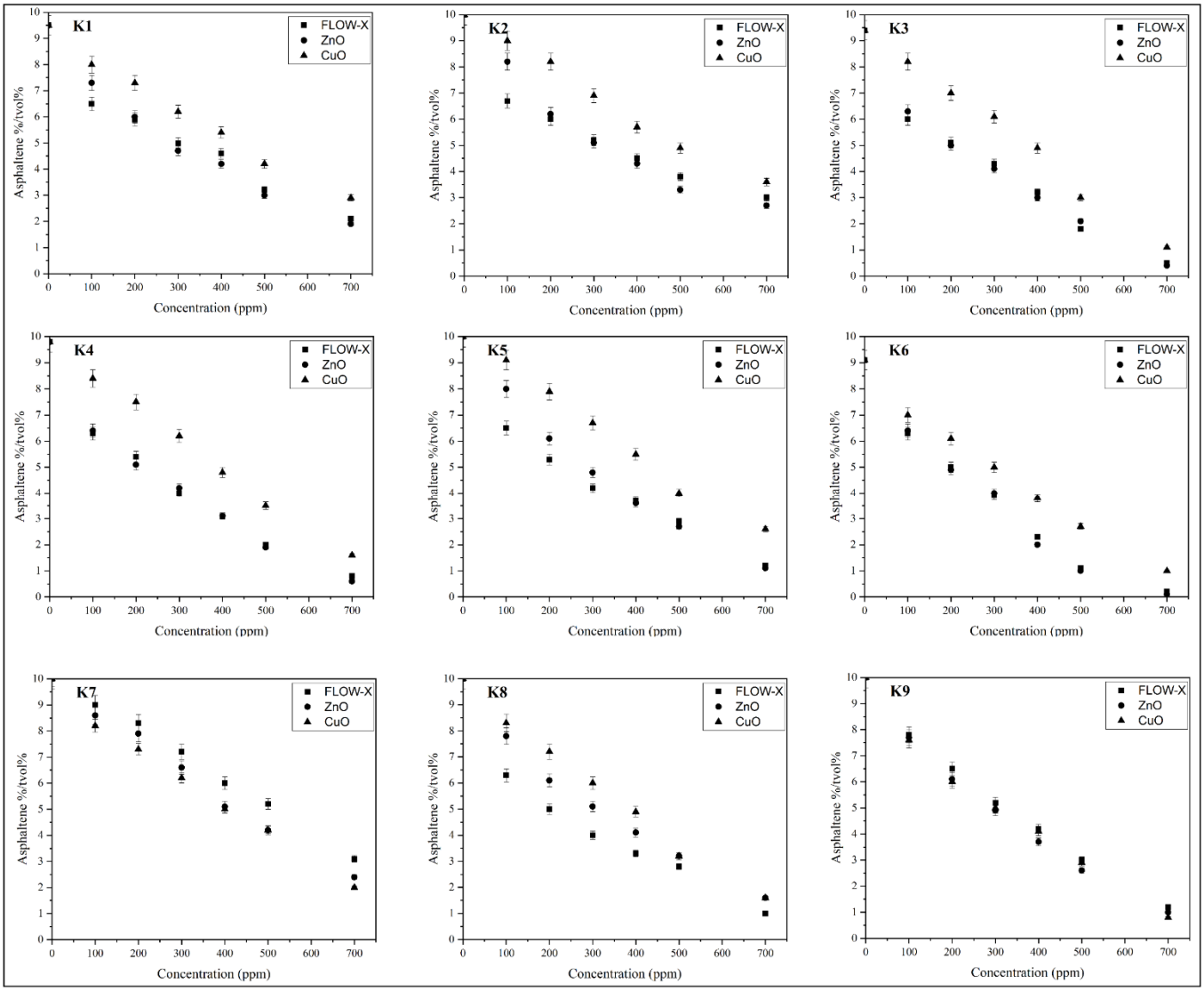

Figure 9. ADT results of K1, K2, and K3–K9 samples.

3.7. ADT Results at 100–700 ppm Doses of Cuo, ZnO, and FLOW-X

Figure 9 shows the results of 100 ppm dosages for the three inhibitors used. It is notable that the commercial inhibitor is effective on most crudes in reducing asphaltene at the initial concentration, while (K9, K7) CuO nanofluids gave the best results in terms of inhibiting asphaltene. Figure 10 shows asphaltene dispersion for each of the samples tested in percentages of the total asphaltene. Some of the important observations are that at a 100 ppm dosage, crude type is the controlling factor, and for each type, certain optimizations need to be considered. At a 200 ppm dosage for the three inhibitors used, it is clear that the green metal nano oxide chemical performs better than the commercial inhibitor in K4, K9, and K7. Some of the important observations noted are that at the 200 ppm dosage, the inhibitor concentration is the controlling factor in reducing the amount of precipitated asphaltene. At the 300 ppm dosage for the three inhibitors used, it is evident that ZnO NF gave better results in terms of reducing or dispersing asphaltene as compared to the other two inhibitors. While for the CuO NF, sample K7 was the most dispersed asphaltene in most of the concentrations. For the 400–700 ppm dosage, ZnO showed the same trend as before in that it had slightly better dispersion than FLOW-X; in some cases of 700 ppm, the difference was almost 20% (K1–K4). From the properties of the tested crudes, it is obvious that the CuO inhibitor was effective on heavy crude samples, whereas for light crudes, ZnO

was better than FLOW-X. Further increasing the concentration would be uneconomical and expensive, which is discussed later in this research. Figure 10 shows asphaltene dispersion for each of the samples tested in percentages of the total asphaltene. Some of the important observations are that at the 700 ppm dosage, the inhibitor reached its potential and no distinct differences can be found above 700 ppm.

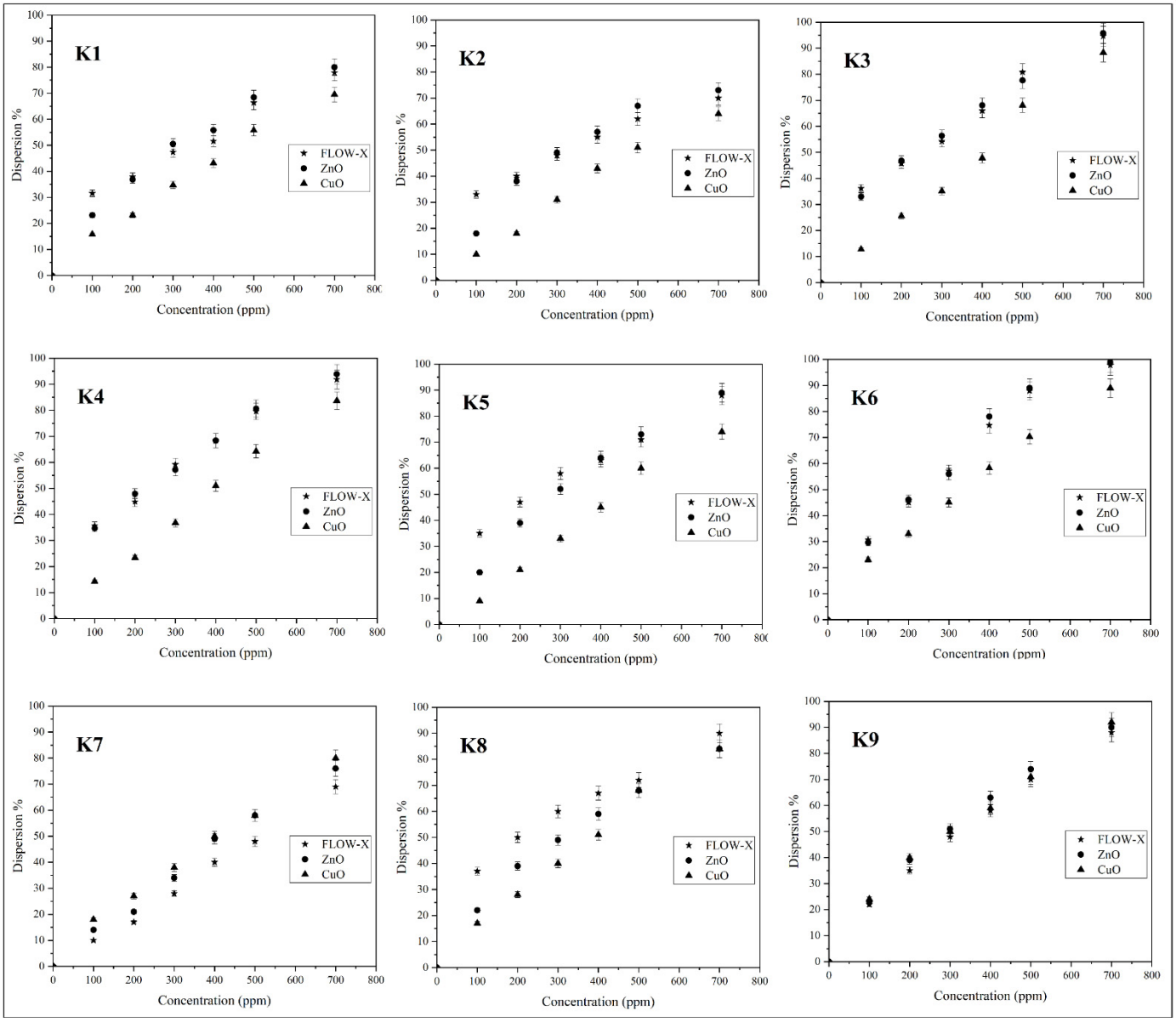

Figure 10. Asphaltene Dispersion percentages at different inhibitor concentrations for (K1–K9).

3.8. Asphaltene Dispersion from UV–Vis Tests

Two crude samples, K3 and K7, were used in order to verify the ADT findings, reliability, and repeatability of this test. First, 0.07 mg/mL of toluene was used to dissolve the isolated asphaltene precipitate. Peaks for K3 and K7 were seen at 286 and 305 nm, respectively. Figure 11 (K3 and K7) shows the absorbance for various inhibitor doses (FLOW-X, CuO, and ZnO NFs).

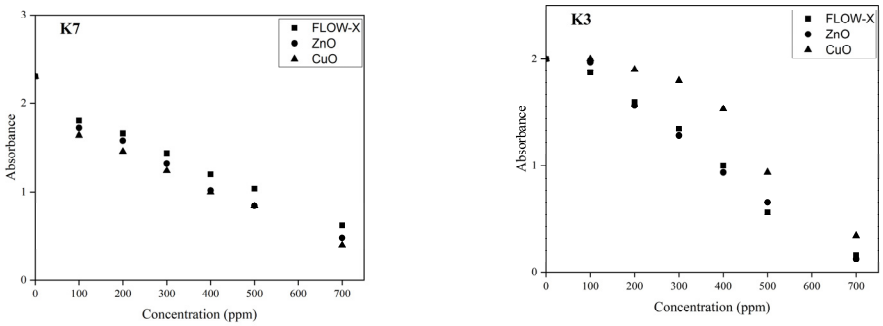

Figure 11. Asphaltene Adsorption by UV–Vis left (K3) right (K7).

3.9. Inhibitor Efficacy and Feasibility of This Research

On the basis of inhibitor concentration in terms of ppm for each of the used chemicals in Table 6, the efficiency of CuO, ZnO, and FLOW-X can be calculated in ppm/dispersed asphaltene% to calculate whether it is feasible to use nano-inhibitors as compared to those commercially available. This calculation is based on the amount of 1 ppm required to disperse a certain amount of asphaltene, which means the lower value is efficient when comparing concentration to concentration of the inhibitors used in this study. The concertation of 400 ppm will be used since it gave the most tangible results. Results show that ZnO nanofluid/chemical is on average 5−22% more effective than commercial inhibitors. The most effective setup per ppm of asphaltene dispersed is ZnO for K6 at 5.1 ppm/1% asphaltene dispersed, and the least effective is FLOW-X for K7 at 10 ppm/1% asphaltene. While CuO showed the worst results, it was the most effective on sample K7.

Table 6. Efficiency 1 ppm of inhibitor to 1% percent of asphaltene dispersion.

Sample	*400/Dis FLOW-X*	*400/Dis ZnO*	*400/Dis CuO*
K1	7.8	7.2	9.3
K2	7.3	7.0	9.3
K3	6.1	5.9	8.4
K4	5.9	5.9	7.8
K5	6.3	6.3	8.9
K6	5.4	5.1	6.9
K7	10.0	8.2	8.0
K8	6.0	6.8	7.8
K9	6.9	6.3	6.8
Average	6.8	6.5	8.1

4. Discussion

Many scholars have studied asphaltene adsorption into nanoparticles. The authors in [26] found that synthesized calcium oxide nanoparticles have a greater adsorption capacity than silicon dioxide. While [13] showed that CaO nanoparticles reduced asphaltene precipitation during a reduction in pressure. The authors in [27] formulated a zirconia–zinc–copper nanocomposite and found greater absorption levels than for zirconia alone. The results of the ADT test are completely in line and confirm what the literature has found. The confirmation of ADT tests by using UV–Vis also adds to the finding of this research that metal oxide nanoparticles exhibit a higher adsorption capacity. Below are some key points of discussion.

- Control tests for ADT were kept at 10% asphaltene for all samples, which can give precise measurements and a good baseline indicator to compare the results of each inhibitor of this research to each other.
- ADT is a simple and well-documented test and can be used in oil field trials to monitor inhibitor performance.

- At the 100 ppm dosage, the controlling factor was crude oil type in terms of API, Specific gravity, and asphaltene content.
- A 500 ppm dosage of ZnO gave the best result out of the three inhibitors used, while CuO for K7 was very efficient.
- At 100 ppm, FLOW-X was better in inhibiting asphaltene as it is used in oil fields.
- At 700 ppm, there was a negligible improvement, especially for CuO and ZnO NPs, and the advantages of lower ppm outweigh the added cost of increasing the concentration.

5. Conclusions

In the context of this study, nano chemical inhibitors outperformed commercially available inhibitors in terms of improving asphaltene dispersion by a minimum of 5% to 22%. Any inhibitor's ability to work depends on a variety of factors, including (concentration, efficiency, and manufacturing costs). The most effective formulation per concentration of the active solution was the ZnO nanofluid/chemical. UV–Vis tests confirmed the visual ADT findings. The use of nanomaterials, however, increases the extent of asphaltene adsorption, thereby enhancing the inhibitory properties of commercial inhibitors, which work very well. This study adds to the body of evidence showing how effectively and efficiently asphaltene precipitation can be improved by nanotechnology. Some of the main conclusions from this work are listed below.

- The ZnO nanofluid/chemical was the most efficient in terms of concentration per asphaltene dispersion.
- The CuO nanofluid/chemical had the efficiency dispersion percentage of asphaltene at heavy crudes.

Author Contributions: Conceptualization, D.K. and H.S.; methodology, D.K.; validation, H.S.; formal analysis, D.K.; investigation, D.K.; resources, D.K.; data curation, D.K.; writing—original draft preparation, D.K.; writing—review and editing, D.K.; visualization, D.K.; supervision, H.S.; project administration, D.K.; funding acquisition, D.K. All authors have read and agreed to the published version of the manuscript.

Funding: This research received no external funding.

Acknowledgments: I would like to acknowledge the support from Gulf Keystone Petroleum-Erbil.

Conflicts of Interest: The authors declare no conflict of interest.

References

1. Thawer, R.; Nicoll, D.C.A.; Dick, G. Asphaltene Deposition in Production Facilities. *SPE Prod. Eng.* **1990**, *5*, 475–480. [CrossRef]
2. Rivero-Sanchez, J.A.; Ramos-Pallares, F.; Schoeggl, F.F.; Yarranton, H.W. Asphaltene Precipitation from Heavy Oil Diluted with Petroleum Solvents. *Energy Fuels* **2021**, *35*, 9396–9407. [CrossRef]
3. Ahmadi, Y.; Kharrat, R. A Compositional Reservoir Simulation and Experimental Investigation of Asphaltene Onset Pressure. *Pet. Sci. Technol.* **2014**, *32*, 2253–2262. [CrossRef]
4. Soleymanzadeh, A.; Yousefi, M.; Kord, S.; Mohammadzadeh, O. A review on methods of determining onset of asphaltene precipitation. *Journal of Petroleum Explor. Prod. Technol.* **2019**, *9*, 1375–1396. [CrossRef]
5. Doryani, H.; Malayeri, M.R.; Riazi, M. Visualization of asphaltene precipitation and deposition in a uniformly patterned glass micromodel. *Fuel* **2016**, *182*, 613–622. [CrossRef]
6. Madhi, M.; Kharrat, R.; Hamoule, T. Screening of inhibitors for remediation of asphaltene deposits: Experimental and modeling study. *Petroleum* **2017**, 4. [CrossRef]
7. Mohammadi, M.; Dadvar, M.; Dabir, B. TiO_2/SiO_2 nanofluids as novel inhibitors for the stability of asphaltene particles in crude oil: Mechanistic understanding, screening, modeling, and optimization. *J. Mol. Liq.* **2017**, *238*, 326–340. [CrossRef]
8. Hoepfner, M. Investigations into Asphaltene Deposition, Stability, and Structure. 2013. Available online: https://hdl.handle.net/2027.42/100081 (accessed on 15 July 2022).
9. Ahmadi, Y.; Eshraghi, S.E.; Bahrami, P.; Hasanbeygi, M.; Kazemzadeh, Y.; Vahedian, A. Comprehensive Water–Alternating-Gas (WAG) injection study to evaluate the most effective method based on heavy oil recovery and asphaltene precipitation tests. *J. Pet. Sci. Eng.* **2015**, *133*, 123–129. [CrossRef]
10. Kazemzadeh, Y.; Eshraghi, S.E.; Kazemi, K.; Sourani, S.; Mehrabi, M.; Ahmadi, Y. Behavior of Asphaltene Adsorption onto the Metal Oxide Nanoparticle Surface and Its Effect on Heavy Oil Recovery. *Ind. Eng. Chem. Res.* **2015**, *54*, 233–239. [CrossRef]

11. Liu, H.; Jin, X.; Ding, B. Application of nanotechnology in petroleum exploration and development. *Pet. Explor. Dev.* **2016**, *43*, 1107–1115. [CrossRef]
12. Ahmadi, Y. Relationship between Asphaltene Adsorption on the Surface of Nanoparticles and Asphaltene Precipitation Inhibition During Real Crude Oil Natural Depletion Tests. *Iran. J. Oil Gas Sci. Technol.* **2021**, *10*, 69–82.
13. Ahmadi, Y.; Aminshahidy, B. Effects of hydrophobic CaO and SiO_2 nanoparticles on Asphaltene Precipitation Envelope (APE): An experimental and modeling approach. *Oil Gas Sci. Technol.* **2018**, *73*, 56. [CrossRef]
14. Alhreez, M.; Wen, D.; Ali, L. A novel inhibitor for controlling Iraqi asphaltene problems. In Proceedings of the 2017 International Conference on Environmental Impacts of the Oil and Gas Industries: Kurdistan Region of Iraq as a Case Study (EIOGI), Koya-Erbil, Iraq, 17–19 April 2017.
15. Mohammadi, M.; Akbari, M.; Fakhroueian, Z.; Bahramian, A.; Azin, R.; Arya, S. Inhibition of Asphaltene Precipitation by TiO_2, SiO_2, and ZrO_2 Nanofluids. *Energy Fuels* **2011**, *25*, 3150–3156. [CrossRef]
16. Ahmadbaygi, A.; Bayati, B.; Mansouri, M.; Rezaei, H.; Riazi, M. Chemical study of asphaltene inhibitors effects on asphaltene precipitation of an Iranian oil field. *Oil Gas Sci. Technol.* **2020**, *75*, 6. [CrossRef]
17. Aguiar, J.I.S.; Punase, A.; Mazzeo, C. Influence of Asphaltene Inhibitors on Wax and Asphaltene Deposition—Are Problems Associated? In Proceedings of the Offshore Technology Conference Brasil, Rio de Janeiro, Brazil, 29–31 October 2019.
18. Mandal, A.; Deka, B.; Mahto, V.; Nihalani, M.C.; Purohit, S. Synthesis, characterization and evaluation of a novel asphaltene inhibitor to control organic solid deposition in petroleum formation. *Pet. Sci. Technol.* **2019**, *37*, 780–786. [CrossRef]
19. Chen, C.; Guo, J.; An, N.; Pan, Y.; Li, Y.; Jiang, Q. Study of asphaltene dispersion and removal for high-asphaltene oil wells. *Pet. Sci.* **2012**, *9*, 551–557. [CrossRef]
20. Alemi, F.M.; Mohammadi, S.; Dehghani, S.A.M.; Rashidi, A.; Hosseinpour, N.; Seif, A. Experimental and DFT studies on the effect of carbon nanoparticles on asphaltene precipitation and aggregation phenomena. *Chem. Eng. J.* **2021**, *422*, 130030. [CrossRef]
21. Manek, M.B. Asphaltene Dispersants as Demulsification Aids. In Proceedings of the SPE International Symposium on Oilfield Chemistry, San Antonio, TX, USA, 14–17 February 1995.
22. Sayyad Amin, J.; Nikkhah, S.; Zendehboudi, S. A new experimental and modeling strategy to determine asphaltene precipitation in crude oil. *Chem. Eng. Res. Des.* **2017**, *128*, 162–173. [CrossRef]
23. Mertz, C.; Cheynier, V.; Günata, Z.; Brat, P. Analysis of Phenolic Compounds in Two Blackberry Species (Rubus glaucus and Rubus adenotrichus) by High-Performance Liquid Chromatography with Diode Array Detection and Electrospray Ion Trap Mass Spectrometry. *J. Agric. Food Chem.* **2007**, *55*, 8616–8624. [CrossRef]
24. Shiraishi, M.; Inagaki, M. Chapter 10—X-ray Diffraction Methods to Study Crystallite Size and Lattice Constants of Carbon Materials. In *Carbon Alloys*; Yasuda, E.-I., Ingaki, M., Kaneko, K., Endo, M., Oya, A., Tanabe, Y., Eds.; Elsevier Science: Oxford, UK, 2003; pp. 161–173.
25. Saleh, T.A. Chapter 7—Structural characterization of hybrid materials. In *Polymer Hybrid Materials and Nanocomposites*; Saleh, T.A., Ed.; William Andrew Publishing: Norwich, NY, USA, 2021; pp. 213–240.
26. Ahmadi, Y.; Aminshahidy, B. Inhibition of asphaltene precipitation by hydrophobic CaO and SiO_2 nanoparticles during natural depletion and CO_2 tests. *Int. J. Oil Gas Coal Technol.* **2020**, *24*, 394. [CrossRef]
27. Mansouri, M.; Ahmadi, Y.; Jafarbeigi, E. Introducing a new method of using nanocomposites for preventing asphaltene aggregation during real static and dynamic natural depletion tests. *Energy Sources Part A Recovery Util. Environ. Eff.* **2022**, *44*, 7499–7513. [CrossRef]